320 GHz Analog-to-Digital Converter Exploiting Kerr Soliton Combs and Photonic-Electronic Spectral Stitching

D. Fang[(1)], D. Drayss[(2)], G. Lihachev[(3)], P. Marin-Palomo[(1)], H. Peng[(1)], C. Füllner[(1)], A. Kuzmin[(1)], J. Liu[(3)], R. Wang[(3)], V. Snigirev[(3)], A. Lukashchuk[(3)], M. Zhang[(4)], P. Kharel[(4)], J. Witzens[(5)], C. Scheytt[(6)], W. Freude[(1)], S. Randel[(1)], T. J. Kippenberg[(3)] and C. Koos[(1,2)]

[(1)] Institute of Photonics and Quantum Electronics, Karlsruhe Institute of Technology (KIT), Germany; [(2)] Institute of Microstructure Technology, Karlsruhe Institute of Technology (KIT), Germany; [(3)] Institute of Physics, Swiss Federal Institute of Technology Lausanne (EPFL), Switzerland; [(4)] Hyperlight Corporation, Cambridge, MA, USA; [(5)] Institute of Integrated Photonics, RWTH Aachen University, Germany; [(6)] Heinz Nixdorf Institute, University of Paderborn, Germany; dengyang.fang@kit.edu, christian.koos@kit.edu

Abstract *We demonstrate a photonic-electronic analog-to-digital converter (ADC) offering a record-high acquisition bandwidth of 320 GHz. The system combines a high-speed electro-optic modulator with a Kerr comb for spectrally sliced coherent detection and is used for digitizing ultra-broadband data signals*.

Introduction

Ultra-broadband analog-to-digital converters (ADC) are key to a variety of applications in science and industry, ranging from high-speed communications [1] to radar and security and to capturing of ultra-short events in scientific experiments. While BiCMOS or CMOS-based ADC combine compactness and robustness with the inherent scalability of the underlying technology platforms, the acquisition bandwidths of these devices are limited to typically less than 50 GHz with sampling rates of less than 150 GSa/s [1], [2]. The bandwidths of individual ADC can be increased by electronic time-domain or frequency-domain multiplexing, thereby parallelizing up to four ADC and offering overall acquisition bandwidths of up to 110 GHz with an effective number of bits (ENOB) of approximately 5 [3]. However, the bandwidth-scalability of electronically multiplexed schemes is limited by the analog multiplexer circuits and by the jitter of the associated RF oscillators [4]. Photonic-electronic ADC may overcome some of these limitations [5], [6], exploiting, e.g., optical time-domain sampling through pulse trains from ultra-stable mode-locked fiber lasers. However, these lasers are usually bulky, which prevents integration into miniaturized systems, and they have low repetition rates of the order of 1 GHz, which limits the sampling rate to, e.g., 2.5 GSa/s [5].

In this paper, we demonstrate an ultra-broadband photonic-electronic ADC that exploits an integrated Kerr soliton frequency comb for spectral multiplexing in the optical domain. Our scheme relies on a high-speed electro-optic (EO) modulator that first converts the analog electrical waveform to an optical signal. This signal is decomposed into spectrally sliced tributaries, which are coherently detected using the phase-locked tones of a Kerr comb as local oscillators (LO). The resulting electronic signals are then spectrally stitched by digital signal processing (DSP) to reconstruct the initial analog waveform. For precise signal reconstruction, we developed a dedicated system model that accounts for the exact complex-valued transfer functions of the various slicing filters and the subsequent in-phase / quadrature (IQ) receivers as well as for the transfer function of the EO modulator. In a proof-of-concept experiment, we demonstrate an implementation with four spectral slices and an overall acquisition bandwidth of 322 GHz. The system offers an estimated ENOB of approximately 2.3, which may be improved to approximately 3.3 by using an optimized LO comb with a higher optical carrier-to-noise ratio (OCNR). We demonstrate the viability of our concept by digitizing sinusoidal signals up to 318 GHz and by acquiring a broadband analog data signal, consisting of a 30 GBd 32QAM waveform centered at 24.4 GHz, a 40 GBd QPSK waveform centered at 233.4 GHz, and a 10 GBd 16QAM waveform centered at 264.4 GHz. To the best of our knowledge, this is the first demonstration of an ADC that relies on detecting spectral slices in the optical domain, leading to the largest acquisition bandwidth demonstrated for any ADC so far.

Concept and implementation

The concept and the experimental setup of the spectrally sliced photonic-electronic ADC are illustrated in Fig. 1. The ultra-broadband analog electrical signal (“Analog In”) is first modulated onto an optical carrier using a high-speed Mach-Zehnder modulator (MZM), see Fig. 1(a). An optical demultiplexer (DEMUX1) with steep roll-off is then used to decompose the ultra-broadband optical waveform into a series of spectral slices that overlap slightly to facilitate spectral stitching in the DSP, similar to the optical arbitrary waveform measurement (OAWM) schemes described in [7], [8]. The spectral slices are then coherently detected by an array of in-phase/quadrature receivers (IQR). The associated local oscillator (LO) tones are derived from a chip-scale soliton frequency comb generator (FCG), pumped by the same laser (L1) that also feeds the MZM such that the optical carrier and all LO tones are strictly phase-correlated. The I and Q components of the signal slices are digitized by an array of synchronized electronic ADC. In the DSP, the digitized signals are frequency-shifted and then stitched together to obtain the desired digital representation of the ultra-broadband analog input. In this stitching process, redundant information contained in the spectral overlap region is used to estimate the relative phase of neighboring slices [8]. In addition, the frequency-dependent complex-valued transfer functions of the various detection channels are compensated based on an initial calibration measurement using a known optical reference signal. Figure 1(b) illustrates the ultra-broadband optical waveform (A, first row), which is sliced into a series of tributaries (second, third, and fourth row) along with the multi-wavelength LO (B, last row). Note that the slice width corresponds to twice the free spectral range f_{FSR} of the LO comb and that only odd-order tones #1, #3, ..., #2*N*-1 are used for coherent reception to ensure gapless signal acquisition from DC to $2N \cdot f_{FSR}$.

Experimental setup and signal reconstruction

To demonstrate the viability of the proposed ADC scheme, we perform a proof-of-concept experiment with four optical detection channels, see Fig. 1(c) for the setup. An external-cavity laser (ECL 1) generates the

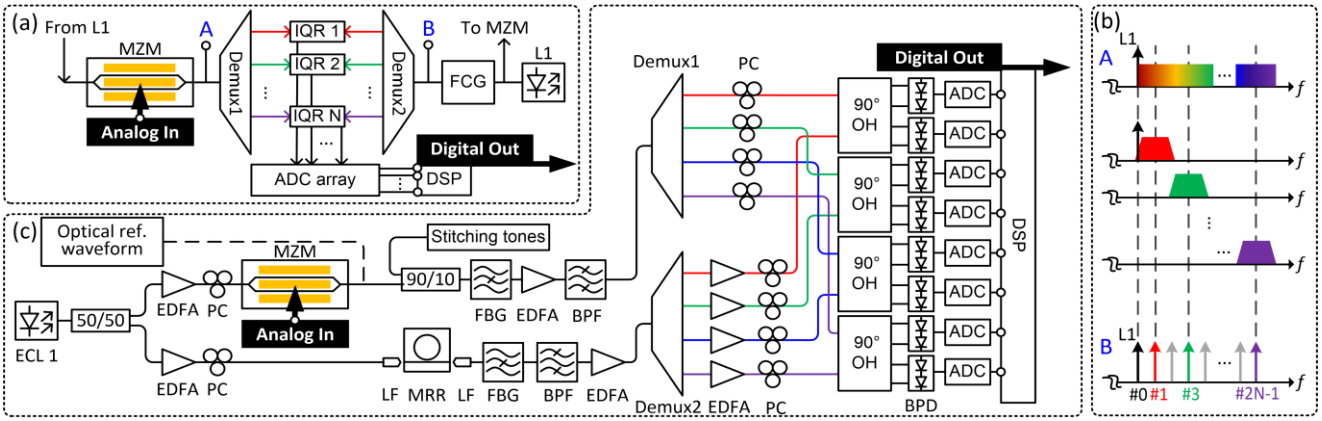

Fig. 1: Concept and experimental setup of the ultra-broadband spectrally-sliced photonic-electronic ADC. **(a)** Concept. The analog electrical signal ("Analog In") is modulated on an optical carrier using a high-speed Mach-Zehnder modulator (MZM) biased in the null point. The resulting optical waveform is then decomposed into a series of spectral slices, which are coherently detected by an array of IQ receivers (IQR). The LO tones are derived from a soliton frequency comb generator (FCG), pumped by the same laser (L1) that also feeds the MZM. The I and Q components of the signal slices are digitized by an array of synchronized electronic ADC. The ultra-broadband waveform ('Digital Out') is then reconstructed by DSP. **(b)** Spectral scheme. Top row: Broadband spectrum at Point A in Fig. 1(a). Row 2 – 4: Overlapping spectral slices. Bottom row: FCG output spectrum at point B in Fig. 1(a). Note that Demux2 selects only the odd comb lines #1, #3 ... #7, which are separated by twice the free spectral range f_{FSR} of the comb. Line #0 is supplied by ECL 1 in Fig. 1(c). **(c)** Experimental setup. Pump laser ECL 1 provides the carrier for the MZM and acts as a pump for the FCG, realized by a Si_3N_4 microring resonator (MRR, see inset; f_{FSR} = 40.25 GHz. Demux1,2 feed a bank of coherent optical receivers with balanced photodetectors (BPD) and 90° optical hybrids (OH). The BPD outputs are AD converted for offline DSP to reconstruct the analog input signal. The slice width amounts to $2f_{FSR}$ = 80.5 GHz.

carrier for the MZM, which is biased in the null point. ECL 1 also serves as a pump for the Kerr comb source, which is based on a high-Q Kerr-nonlinear silicon-nitride micro-resonator operated in the single-soliton regime [9,10] with a free spectral range of f_{FSR} = 40.25 GHz. Wave shapers (WS) are used to spectrally slice the ultra-broadband optical signal and the comb, and an array of four IQ receivers, each comprising a 90° optical hybrid (OH) and a pair of balanced photodetectors, are used for coherent reception. The resulting electrical signals are digitized by eight synchronized channels of two high-speed real-time oscilloscopes (Keysight UXR series). In this experiment, the electrical input signal is modulated onto the optical carrier by a broadband thin-film lithium-niobate ($LiNbO_3$) MZM. Such devices withstand high optical powers and can reach 3 dB bandwidths of up to 100 GHz, while still showing a reasonable modulation response well beyond 300 GHz [10], [11]. An alternative option could be ultra-broadband hybrid devices that combine silicon photonic or plasmonic waveguides with organic electro-optic materials [12-16]. The exact transfer function of the MZM is measured using a technique similar to the one described in [13] and then compensated for by the DSP.

For digital reconstruction, the recorded signal slices are numerically frequency-shifted according to the spacing of the LO comb tones and then merged. To this end, we consider our receiver array as a single-input multiple-output (SIMO) system and use maximal-ratio combing (MRC) [17] to maximize the SNR of the combined waveform. Importantly, for proper reconstruction, the complex-valued transfer functions of the associated optoelectronic signal paths between the MZM output and the electronic ADC outputs need to be measured and considered in the DSP. To this end, we first separate each transfer function into two components: A time-invariant frequency-dependent part, representing the characteristics of the demultiplexer, the associated filters, the erbium-doped fiber amplifiers (EDFA), and the receiver, and a slowly varying frequency-independent complex-valued factor, that accounts for the amplitude and phase fluctuations of the comb lines as well as for the random phase drift in the fibers. For precisely measuring the time-invariant part, we use a novel one-time calibration method that relies on feeding the system with a known optical reference waveform generated by an ultra-stable mode-locked laser (MENHIR-1550, rep. rate 250 MHz, pulse width 200 fs), see Fig. 1(c). The amplitude and phase spectrum of this signal are obtained by an independent frequency-resolved optical gating (FROG) measurement. By comparing the received spectra at the detector outputs with the known spectrum of the reference waveform, we derive the time-invariant transfer functions. For estimating the slowly varying path-dependent factors, we correct for the time-invariant transfer functions first and then compare the complex-valued amplitude spectra in the overlap regions between adjacent slices.

ENOB estimation and functional demonstration

To prove the viability of our concept, we use the setup shown in Fig. 1(c) to record different electronic signals, see Fig. 2. Figure 2(a) shows the measured amplitude and phase of the complex-valued transfer functions of the four optical channels as used for signal reconstruction. In a first set of experiments, we use sinusoidal test signals with different frequencies, see Fig. 2(b) for the corresponding results. The 40 GHz signal was obtained from a radio-frequency (RF) synthesizer, whereas the 242.5 GHz- and the 317.6 GHz-signal were generated by beating two laser tones (intrinsic linewidth < 5 kHz) on a high-speed uni-travelling carrier (UTC) photodiode. In these experiments, we artificially added optical "stitching tones" in the spectral overlap range of adjacent slices, see Fig. 1(c). This ensures proper stitching of the slices even in absence of spectral content of the use signal in the overlap regions. Upon reconstruction of the signal, the stitching tones can be removed by DSP. The red lines in Fig. 2(a) correspond to the reconstructed waveform, which were obtained from a sinc-type interpolation of the measured sampling points (green circles). The blue traces correspond to a sinusoidal least-squares fit of the measured time-domain data. All signals were recorded for over 15.6 µs – short enough to avoid phase walk-off due to non-zero laser

978-1-6654-3868-1/21/$31.00 ©2021 IEEE

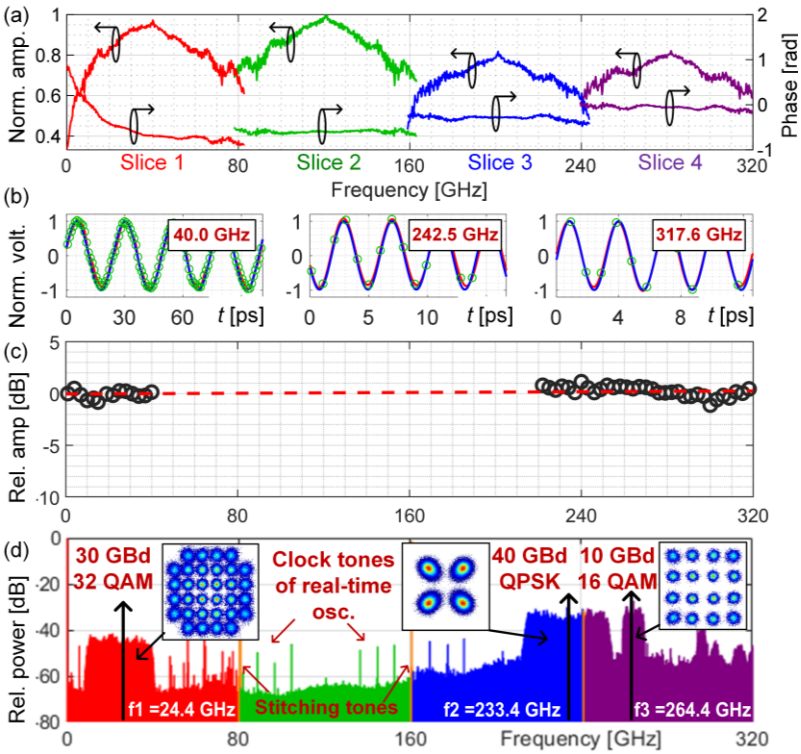

Fig. 2: ADC demonstration. **(a)** Amplitude and phase of the complex-valued transfer functions of the four detection channels as obtained from the calibration measurement. **(b)** Acquired sinusoidals at 40 GHz, 242.5 GHz, and 317.6 GHz. Green circles: Sampling points. Red curve: Sinc-interpolation of the sampling points. Blue curve: Fitted sinusoidal. **(c)** Frequency response of the ADC system upon compensation of the MZM transfer function. Black circles: Measured data points; dashed red line: Linear fit. The frequency response is essentially flat over the full bandwidth of 320 GHz. **(d)** Stitched spectrum of a superposition of three QAM signals, centered at carrier frequencies f_1, f_2, f_3 along with the corresponding constellation diagrams. Overlap regions and stitching tones are indicated in orange.

linewidths for the optically generated test signals. The measured and the fitted waveforms show good agreement, even for the tone at 242.5 GHz, which is within the spectral overlap region of Slices 3 and 4, thus confirming the viability of the stitching concept.

We also estimate the ENOB of our system, which quantifies the signal-to-noise-and-distortion ratio (SINAD) of a harmonic test signal that fully covers the ADC acquisition, ENOB = ($\mathrm{SINAD_{dB}}$-1.76) / 6.02, where $\mathrm{SINAD_{dB}}$ refers to the SINAD measured in dB [18]. For our scheme, the acquisition range is limited by the nonlinear transfer characteristics of the MZM. For a quantitative analysis, we measure the noise power of our system and then calculate the peak-to-peak drive voltage $U_{\mathrm{max,pp}} \approx 0.70\ U_{\pi} = 1.68$ V for which the third-order intermodulation products reach the same power level as the system noise when operating the MZM with a low-frequency sinusoidal. This voltage corresponds to the acquisition range of our ADC. To estimate the ENOB, we drive the system with a sinusoidal signal at 309 GHz. Lacking a signal source that can generate a full-range signal with a peak-to-peak voltage of $U_{\mathrm{max,pp}} = 1.68$ V at 309 GHz, we use a smaller amplitude, extract the distortions, and then estimate a SINAD of 15.7 dB (ENOB of 2.3), which can be expected for a full-range sinusoidal. We find that the SINAD is strongly limited by the rather low optical carrier-to-noise ratio (OCNR) of the LO comb, which amounts to only 22.6 dB for a noise reference bandwidth of 12.5 GHz (0.1 nm). For optimized Kerr combs, OCNR in excess of 40 dB are not unusual [19]. This would lead to a SINAD of at least 21.6 dB (ENOB = 3.3) without considering any further reduction of other noise contributions. Note that the time base of the current system still relies on the RF oscillators of the oscilloscopes such that the ENOB will still be limited by the associated timing jitter. Note also that we neglected the optical stitching tones and the impact of the electronic ADC noise in our ENOB analysis.

To investigate the spectral characteristics of our ADC, we acquire sinusoidal tones at various frequencies and refer the digitally recorded signal power to the power of the respective analog signals. The resulting transfer function is normalized to its value in the low-frequency limit, see Fig. 2(c). Note that we could not record any signals between 50 GHz and 220 GHz due to the lack of adequate sources. Still, the measurement shows that the ADC offers an essentially flat frequency response up to 320 GHz. In a final set of experiments, we use the system to acquire a broadband analog data signal, consisting of a 30 GBd 32QAM waveform centered at 24.4 GHz, a 40 GBd QPSK waveform centered at 233.4 GHz, and a 10 GBd 16QAM waveform centered at 264.4 GHz. Figure 2(d) shows the spectrum along with the constellation diagrams of the various data signals. The increase of the noise floor towards higher frequencies and the noise peaks around 297 GHz are a consequence of the compensation of the MZM transfer function, which decays continuously with frequency while featuring some dips around 297 GHz. Note that, in this experiment, the ultra-broadband data signal could not be fed to the MZM through a single probe due to the large electrical bandwidth. We therefore used a second set of electrodes of the MZM to supply the 30 GBd 32QAM signal at 24.4 GHz. Besides the data signals, the spectrum contains residual clock tones of the oscilloscope as well as stitching tones at approximately 80.5 GHz and 161.0 GHz. Overall, the signals were reconstructed with acceptable quality, thereby proving the viability of the scheme.

Summary

We demonstrated a photonic-electronic ADC with a record-high acquisition bandwidth of 320 GHz. The concept relies on an EO modulator for converting the analog electrical waveform to an optical signal, which is spectrally sliced and coherently detected using a Kerr frequency comb as a multi-wavelength LO. From our experiments, we estimate an ENOB of approximately 2.3, which may be further improved to 3.3 by reducing the OCNR of the LO Kerr comb. The viability of the scheme is demonstrated in proof-of-concept experiments using ultra-broadband data signals. To the best of our knowledge, this is the first demonstration of an ultra-broadband ADC that relies on spectral slicing in the optical domain. By increasing the number of slices and by exploiting highly stable Kerr combs with ultra-low phase noise [20], our concept may open a path to acquisition bandwidths of the order of 1 THz using a fully integrated photonic-electronic system [8].

978-1-6654-3868-1/21/$31.00 ©2021 IEEE

Acknowledgements
This work was supported by the ERC Consolidator Grant TeraSHAPE (no. 773248), by the H2020 project TeraSlice (# 863322), by the H2020 Marie Skłodowska-Curie Innovative Training Network "MICROCOMB" (# 812818), by the Deutsche Forschungsgemeinschaft (DFG) project PACE (no. 403188360) within the Priority Programme "Electronic-Photonic Integrated Systems for Ultrafast Signal Processing" (SPP 2111), by the Alfried Krupp von Bohlen und Halbach-Stiftung, and by the Max-Planck School of Photonics (MPSP). The work relies on instrumentation funded by the European Regional Development Fund (ERDF, grant EFRE/FEIH_776267), the Deutsche For-schungsgemeinschaft (DFG; grants DFG/INST 121384/166-1 and DFG/INST 121384/167-1. The Si3N4 samples were fabricated in the Center of MicroNanoTechnology (CMi) at EPFL.

References

[1] T. Drenski and J. C. Rasmussen, "ADC & DAC - Technology Trends and Steps to Overcome Current Limitations," *OFC 2018*, paper M2C.1.
[2] A. Zandieh *et al.*, "A 2x-Oversampling, 128-GS/s 5-bit Flash ADC for 64-GBaud Applications," *BCICTS 2018*, pp. 52-55.
[3] Keysight Technologies, Infiniium UXR-Series Oscilloscopes. https://www.keysight.com/us/en/assets/7018-06242/data-sheets/5992-3132.pdf
[4] G. Valley, "Photonic analog-to-digital converters", *Opt. Expr*. 15, 1955-1982 (2007)
[5] A. Khilo *et al.*, "Photonic ADC overcoming the bottleneck of electronic jitter," *Opt. Expr*, 20, 4454–4469 (2012).
[6] A. Zazzi *et al.*, "Fundamental limitations of spectrally-sliced optically enabled data converters arising from MLL timing jitter," Opt. Expr. 28, 18790–18813 (2020).
[7] N. K. Fontaine *et al.*, "Real-time full-field arbitrary optical waveform measurement," *Nature Photon.* 4, 248–254 (2010).
[8] D. Fang *et al.*, "Optical arbitrary waveform measurement on the silicon photonic platform," *OFC 2021*, paper F2E.6.
[9] Herr, T. *et al.* Temporal solitons in optical microresonators. *Nature Photon.* 8, 145–152 (2014).
[10] C. Wang *et al.*, "Integrated lithium niobite electro-optic modulators operating at CMOS-compatible voltages," *Nature* 562, 101–104 (2018).
[11] A. J. Mercante *et al.*, "Thin film lithium niobate electro-optic modulator with terahertz operating bandwidth," *Opt. Expr.* 26, 14810-14816 (2018)
[12] M. Burla *et al.* "500 GHz plasmonic Mach-Zehnder modulator enabling sub-THz microwave photonics", APL Photonics 4, 056106 (2019)
[13] S. Ummethala *et al.*, "THz-to-optical conversion in wireless communications using an ultra-broadband plasmonic modulator," *Nature Photon.* 13, 519–524 (2019).
[14] S. Ummethala et al., "Hybrid electro-optic modulator combining silicon photonic slot waveguides with high-k radio-frequency slotlines," *Optica* 8, 511-519 (2021)
[15] H Zwickel et al., "Verified equivalent-circuit model for slot-waveguide modulators," *Opt. Expr.* 28, 12951-12976 (2020).
[16] C. Kieninger *et al.*, "Silicon-organic hybrid (SOH) Mach-Zehnder modulators for 100 GBd PAM4 signaling with sub-1 dB phase-shifter loss," *Opt. Expr.* 28, 24693-24707 (2020)
[17] D. G. Brennan, "Linear Diversity Combining Techniques," *in Proc. of the IEEE*, 91, 331-356 (2003).
[18] "IEEE Standard for Terminology and Test Methods for Analog-to-Digital Converters," in IEEE Std 1241-2010 (Revision of IEEE Std 1241-2000) , vol., no., pp.1-139, 14 Jan. 2011, doi: 10.1109/IEEESTD.2011.5692956.
[19] P. Marin-Palomo, J. Kemal, M. Karpov *et al.* "Microresonator-based solitons for massively parallel coherent optical communications," *Nature* 546, 274–279 (2017)
[20] J. Liu *et al.*, "Photonic microwave generation in the X- and K-band using integrated soliton microcombs," *Nature Photon.* 14, 486–691 (2020).